Mechanism and Machine Theory 145 (2020) 103716

Contents lists available at ScienceDirect

Mechanism and Machine Theory

journal homepage: www.elsevier.com/locate/mechmachtheory

Research paper

Dynamic modelling and optimal design of a clutch actuator for heavy-duty automatic transmission considering flow force

Tiancheng Ouyang[a,b,*], Guicong Huang[a], Shuoyu Li[a], Jingxian Chen[a], Nan Chen[b]

[a] College of Mechanical Engineering, Guangxi University, Nanning, PR China
[b] School of Mechanical Engineering, Southeast University, Nanjing, PR China

ARTICLE INFO

Article history:
Received 16 October 2019
Revised 14 November 2019
Accepted 17 November 2019
Available online xxx

Keywords:
Heavy-duty automatic transmission
Clutch actuator
Dynamic modelling
Artificial bee colony algorithm
Optimal design

ABSTRACT

With the rapid development of heavy-duty vehicles, increasing attention has been paid to the performance of high-power automatic transmission. An electro-hydraulic actuator, as a key component in automatic transmission, is crucial to the shifting quality. In this study, we develop a dynamic model of an electro-hydraulic actuator for heavy-duty vehicles, and adopt the artificial bee colony (ABC) algorithm to optimize the structural parameters to improve the ride comfort and fuel economy. First, a detailed model considering the flow force is developed to describe the motion inside the actuator based on the theory of fluid dynamics. Then the key design parameters, which affect the shifting performance significantly, are identified by combining the Bode plots and sensitivity analysis. Finally, the electro-hydraulic actuator is optimized to ensure the actual curve approximates the ideal trajectory while shortening the clutch pressure response time maximally by using the ABC algorithm. In comparison with the original parameters, the optimized design shows a major improvement in the rapid response and precise control of gear shifting. This investigation provides an efficient approach to design the structure parameters of clutch actuators to increase their shifting performance.

1. Introduction

Transmission, as a process to regulate different engine speeds and torques, is indispensable in a vehicle [1,2]. With the development of the vehicle technology, the traditional manual transmission is already unable to satisfy the demand of consumers because of the complex shifting process. Thus, engineers have provided automatic transmission as a solution to simplify the operation of shifting, relieve the fatigue of drivers, and decrease the fuel consumption [3–5]. Currently, hydraulic automatic transmission (AT) and continuously variable transmission (CVT) are the most well-known approaches in passenger vehicles [6,7]. With rapid increase in the number of heavy-duty vehicles, there is a pressing need to adopt AT. For small-displacement vehicles, CVT is better than AT owing to the continuous and smooth power transmission; however, the drive belt in CVT cannot endure the power with regard to heavy-duty vehicles [8]. Hence, AT is much better than CVT for improving the drive comfort. Because the engaging and separating processes between clutches mainly depend on the clutch pressure in AT, the clutch pressure is critical to the performance of shifting. Therefore, controlling the clutch pressure

* Corresponding author at: College of Mechanical Engineering, Guangxi University, Nanning, PR China.
E-mail address: ouyangtiancheng@gxu.edu.cn (T. Ouyang).

https://doi.org/10.1016/j.mechmachtheory.2019.103716
0094-114X/

precisely and decreasing the time delay with an electro-hydraulic actuator in heavy-duty vehicles have been the priority areas for research [9–11].

An electro-hydraulic actuator used for the automatic transmission in heavy-duty vehicles, is mainly composed of three parts: a proportional solenoid valve (PSV), a pressure reducing valve (PRV), and clutch actuator. A PSV, as a pilot device controlling the movement of a PRV, is typically used to regulate the clutch pressure indirectly [12]. Numerous studies have focused on the signal control of the PSV [13–15]. However, governing only the PSV cannot meet the objects of rapid response and precise control. The structure of a PRV is also important owing to its excellent transient response and self-lubricating property. Numerous researchers have built accurate models to analyse the dynamic performance of a PRV and worked on its optimal design [16–18]. To overcome the challenge of spool clamping caused by the excess flow force, several structures were designed based on the model of a PRV considering the flow force in [19]. In [20], a type of novel PRV with an orifice plate was introduced, and the temperature and energy loss were simulated with the change in geometric features of the PRV. For a three-way PRV, He et al. [21] believed that a damping orifice with a diameter of 0.5 mm and a throttle with four round holes could obtain the best dynamic performance at low pressures. Moreover, Gad [22] also deemed that the size of the throttling orifice had a tremendous influence on the performances of the steady state and transient operations. Furthermore, the main reason for the non-linear characteristic is the variation in transient operation in a PRV. The above-mentioned investigations indicated the importance of the flow environment. In fact, the flow rate of a fluid is high level particularly in the process of shifting, implying that the flow force is sufficiently large in heavy-duty vehicles. Such a high flow crossing to a PRV will probably majorly disturb the whole system [23]. Hence, the structure design and parameter optimization of PRVs is extremely significant.

To identify the design variables in the optimization, approaches, such as empirical judgement based on fuzzy logic, sensitivity analysis and analysis of variance are frequently adopted in engineering fields. In [24], the authors assessed and optimized the parameters of a rail vehicle by using a fuzzy logic expert system. The study in [25] applied sensitivity analysis to identify the factor impacting the output of the model. Chen et al. [26] also determined the essential geometrical parameters of the displacement amplification mechanism using global sensitivity. Additionally, in [27,28], the analysis of variance was utilized to determine which variables were crucial. Another study identified the relative factors by comparing the results of the analysis of variance and an empirical model [29].

It is essential to use an appropriate optimization method for the problem of structure and parameter design. Aiming at passenger comfort under different load cases, Haj-Fraj and Pfeiffer [30] employed the sequential quadratic programming (SQP) method to optimize the power train during the automatic transmission. In [31], the structure of a PSV was optimized to accelerate the response of the gear shift by using a multi-island genetic algorithm (MIGA). Similarly, Amirante et al. [32] employed a genetic algorithm (GA) to redesign the structure of the hydraulic proportional directional spool to decrease the flow force. Compared to the simplex algorithm, the optimization results were better with the GA when the valve moved to the maximum position in the study. In [33], a non-linear mathematical model was proposed for a pressure control valve. After stability analysis of the system, the key parameters of the valve were optimized based on the particle swarm optimization algorithm. Although the above-mentioned methods obtained satisfactory results, they consumed a significant amount of time for optimization. In [34], the artificial bee colony (ABC) algorithm was first proposed, whose efficiency of the convergence speed has been validated by comparing to the algorithms in [35,36]. Besides, Li et al. [37] optimized a fibre reinforced plastic ship structure by the ABC algorithm and obtained satisfactory results. Consequently, this study adopts the ABC algorithm to optimize the structure of a PRV and clutch actuator.

Numerous studies have contributed immensely to the improvement of the shifting quality for electro-hydraulic actuators. However, the existing works concentrate on the adjustment of the pilot pressure for the PSV, establishment of a novel model of the PRV, and the optimization of structure parameters of the PSV and PRV for heavy-duty vehicles. They do not consider the clutch actuator in the optimization design. Furthermore, for simplification, the flow force is frequently ignored in dynamic models. Thus, a large error is introduced in the response time under an actual high-flow condition. Once the response time is delayed significantly, the shifting is abrupt, and this causes discomfort to the driver. To solve the above difficulty, first, an accurate model considering flow force is proposed. Then the effects of the structure parameters, including the clutch actuator, are identified and ranked based on Bode plots. Moreover, sensitivity analysis is performed to confirm the results obtained from the Bode plots. Based on the parameter analysis results, the conventional SQP method and a novel ABC algorithm are employed to optimize the structure parameters. The optimization result with the ABC yields a better time response and is far closer to the ideal trajectory than those obtained with the SQP. This demonstrates that an evolutionary optimization algorithm is more suitable than the conventional method for solving such problem. In addition, the curves of the jet angle and discharge coefficient are fitted based on computational fluid dynamics (CFD) simulation of the PRV. It can be regarded that combining ABC algorithm with Bode plots is an effective approach to redesign the structure parameters for improving the shifting comfort.

The remainder of this paper is organized as follows. Section 2 introduces the principle of electro-hydraulic actuator. The dynamic model of the actuator considering the flow force is described in Section 3. Based on the model, the identification and rankings of the influential parameters by the Bode plots and verification of the results via sensitivity analysis are presented in Section 4. In Section 5, the constraint conditions, objective function built in the specific environment are provided. Based on the problem description, the ABC algorithm and SQP method are used to optimize the model respectively. These results are compared and analyzed. Subsequently, in Section 6, the analyses and optimization results are discussed in detail. According to the analysis, several conclusions are drawn in Section 7.

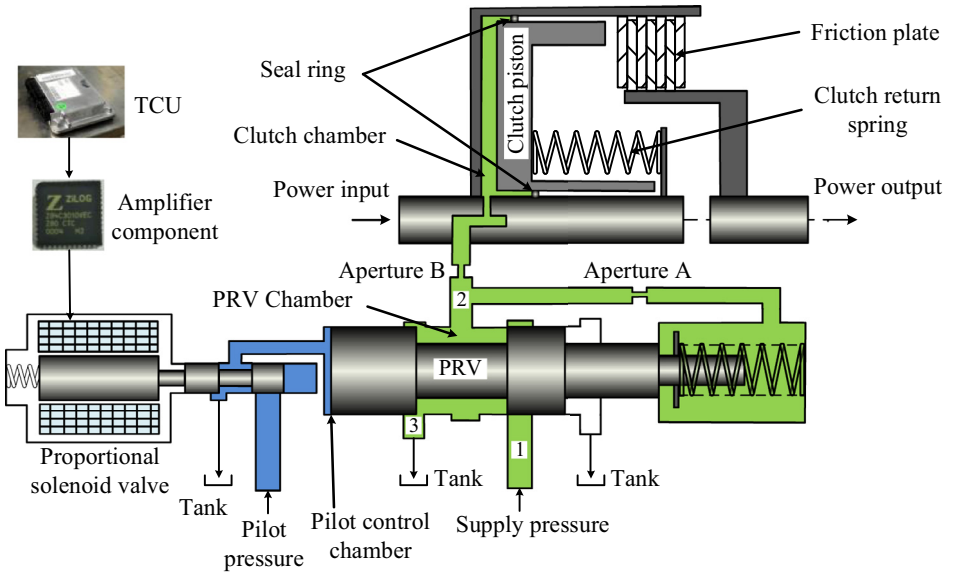

Fig. 1. Schematic diagram of electro-hydraulic actuator.

2. Description of electro-hydraulic actuator

To comprehend the research purposes of this study, the structure and operation principle of an electro-hydraulic actuator are introduced briefly in this section.

An electro-hydraulic actuator, controlling the shift process in automatic transmission, consists of a control unit, proportional solenoid valve (PSV), pressure reducing valve (PRV) and clutch actuator, as presented in Fig. 1. When the driver upshifts, the transmission control unit (TCU) transmits some signals, expanded by the amplifier component, to the PSV to regulate the pilot pressure in the pilot control chamber. With the increasing of pilot pressure, the PRV is impelled to the right to open pipe 1, so that the fluid can flow into the PRV chamber from the supply pressure inlet. A large amount of fluid crosses pipe 2 into the clutch chamber to propel the clutch piston sliding to eliminate the free clearance between the friction plates. The leaking fluid flows back to the oil tank across pipe 3. Finally, the torque is transmitted to the output shaft when the friction plate joints close. The downshifting process is similar to that of the upshifting process, except that the PRV and clutch piston move in opposite directions. It is worth mentioning that engaging/separating the oncoming clutch and off-going clutch simultaneously is conducive to transmit power smoothly; hence, controlling the clutch pressure in a rapid and precise manner is necessary for comfortable gear shifting.

3. Dynamic modelling of electro-hydraulic actuator

For the purpose of describing the motion and performance of an electro-hydraulic actuator accurately, in this section, the dynamics models, comprising of a PSV, a PRV and clutch actuator, are established.

3.1. Simplified solenoid valve model

The electromagnetic force, generated from the solenoid magnet in a PSV, is related to the input current signals from the TCU, which can adjust the pilot pressure in the PSV continuously. However, the actual dynamic model in the PSV is extremely complex. To simplify modelling, the PSV is typically considered approximately as a linear system. Under this assumption, we adopt the formula in [38,39] to describe the relationship of input signal and output pilot pressure, as given below,

$$P_a = \kappa_1 \tau + \kappa_2 \tag{1}$$

where P_a is the pilot pressure, κ_1 and κ_2 are the equivalent coefficients, and τ denotes the duty ratio. For most problems, Eq. (1) can be calculated efficiently within a certain range of errors.

3.2. Pressure reducing valve model

A PRV, as depicted in Fig. 2, is used to regulate the flow rate of the supply fluid which influences the shifting performance significantly. To reflect the scenario in reality precisely, the modelling of PRVs should be appropriately refined. When

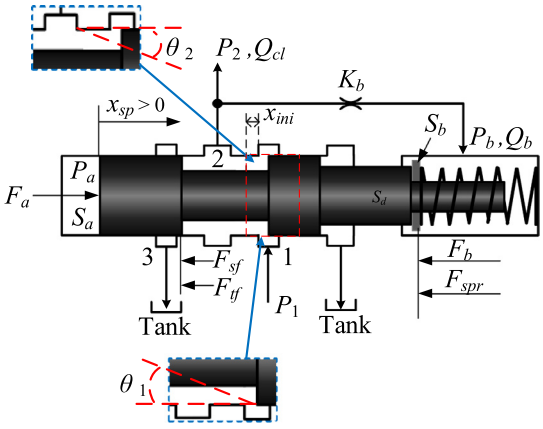

Fig. 2. The structure diagram of the PRV.

the fluid flows across the PRV chamber, a force generating termed as the flow force is generated by the variation in the fluid momentum. Generally, most studies do not consider the flow force owing to the less impact on the balance of the spool under a low flow rate condition. However, the equilibrium may be disturbed by a relatively larger steady flow force, particularly under a high flow rate condition. This suggests that in this case, the PRV cannot be controlled by the PSV as usual, and a self-excited vibration effect may occur. Therefore, it is necessary to consider the flow force under a high flow rate condition. It is assumed that the volume flow and the temperature of the fluid remains constant, and the flow is calculated by a low Reynolds number turbulence model. Based on the above assumptions, the dynamic derivations of the PRV are introduced below.

Pilot force F_a, fluid pressure force F_b, and spring force F_{spr} can be expressed by Eq. (2).

$$\begin{cases} F_a = P_a S_a \\ F_b = P_b S_b \\ F_{spr} = k_{spr}\left(x_{sp} + x_0\right) \end{cases} \tag{2}$$

where P_a and S_a are the pressure and area of the pilot chamber, respectively. P_b and S_b are the pressure and area of the feedback chamber, respectively. k_{spr} is the spring constant, x_{sp} denotes the displacement of the spool, and x_0 represents the initial displacement of the spring when $F_a = 0$.

The flow force can be divided by two types: steady flow force F_{sf} and transient flow force F_{tf}. According to the theorem of momentum, the equation of F_{sf} in the PRV is as follows:

$$F_{sf} = \rho Q_{prv} v_1 \cos\theta_1 - \rho Q_{prv} v_2 \cos\theta_2 \approx \rho Q_{prv} v_1 \cos\theta_1 \tag{3}$$

where ρ is the hydraulic fluid density, Q_{prv} is the flow rate across pipe 1, the velocities of hydraulic fluid passing through pipe 1 and pipe 2 are v_1 and v_2, respectively. The inlet jet angle and outlet jet angle are θ_1 and θ_2, respectively. Since θ_2 is nearly 90°, the latter term in Eq. (3) can be regarded as 0.

By assuming a steady-state, incompressible, flow in a horizontal pipe with negligible frictional losses, flow rate Q_{prv} and flow velocity v_1 are obtained based on Bernoulli's equation as,

$$\begin{cases} Q_{prv} = C_d \pi d_a x_{vo} \sqrt{\dfrac{2\Delta P}{\rho}} \\ v_1 = c_v \sqrt{\dfrac{2\Delta P}{\rho}} \end{cases} \tag{4}$$

where C_d represents the discharge coefficient, d_a is the diameter of the valve, x_{vo} is the opening of pipe 1, ΔP is the pressure difference of the pipes, and c_v is the coefficient of the flow velocity.

Substituting Eq. (4) into Eq. (3), the steady flow force can be described as

$$F_{sf} = 2C_d \Delta P \pi d_a [symb(x_{sp} - x_{ini})] \cos\theta_1 \tag{5}$$

$$symb(x) = \begin{cases} 0 & x < 0 \\ x & x \geq 0 \end{cases} \tag{6}$$

where x_{ini} denotes the overlap of the spool and pipe 1 when the displacement of the spool is $x_{sp} = 0$. Note that the direction of the steady flow force is to close the pipe.

With the motion of the spool, the axial acceleration changes simultaneously resulting in a force termed as the transient flow force that opposes the motion. The transient flow force F_{tf} is expressed as

$$F_{tf} = m_{prv}\dot{v}_1 = \rho A_0 l \frac{d\left(Q_{prv}/A_0\right)}{dt} = C_d \pi d_a \dot{x}_{sp} l \sqrt{2\rho\Delta P} \tag{7}$$

where A_0, m_{prv}, and l represent the longitudinal section area of the PRV, mass of the fluid in the PRV chamber and length of the PRV chamber, respectively. $\dot{x}_{sp}$ is the speed of the spool.

It is assumed that the resistance induced by the viscosity of the oil is approximately proportional to $\dot{x}_{sp}$. Considering the right direction as the positive direction, the dynamic equation is derived as

$$m_e\ddot{x}_{sp} + D_f\dot{x}_{sp} = F_a - F_b - F_{spr} - F_{sf} - F_{tf} \tag{8}$$

Substituting Eq. (2) - (7) into Eq. (8) and introducing the Laplace operator, the equation becomes:

$$\begin{aligned} &P_aS_a - P_bS_b - k_{spr}x_0 + 2C_d\pi d_a(P_1 - P_2)\cos\theta_1 x_{ini} \\ &= m_e s^2 x_{sp} + \left(D_f + C_d\pi d_a l\sqrt{2\rho(P_1 - P_2)}\right)sx_{sp} + (k_{spr} + 2C_d\pi d_a P_1\cos\theta_1)x_{sp} \end{aligned} \tag{9}$$

where P_1 and P_2 denote the pressures of pipe 1 and pipe 2, respectively, m_e is the equivalent mass of the spool whose value equals to a third of the mass of the spring and spool. s and D_f denote the Laplace operator and viscous damping constant, respectively.

The condition of the flow equilibrium is distinct owing to the differences in the flow characteristics under different flow conditions. In the filling state, the spring force, as a resistance force, hinders the motion of the spool. However, in the discharge state, it has an opposite effect, impelling the spool to the original position. Therefore, the establishment of the model should be divided into two processes: filling and discharge. The positive direction is defined as the direction of the spool moving to open pipe 1; hence, the equation of the flow rate for the feedback chamber Q_b during the filling state can be expressed as

$$Q_b = K_b(P_2 - P_b) = \frac{V_b}{\lambda}sP_b - S_bsx_{sp} \tag{10}$$

where K_b is the flow pressure coefficient for feedback damping aperture A, P_2 denotes the pressure of pipe 1, P_b is the pressure of the feedback chamber, V_b is the volume of the feedback chamber, S_b is the area of the feedback chamber, s is the Laplace operator, and the displacement of the spool and effective bulk modulus of the fluid are represented by x_{sp} and λ, respectively.

The volume for the feedback chamber is

$$V_b = V_d - S_bx_{sp} \tag{11}$$

where the initial volume of the feedback chamber is denoted by V_d.

On the basis of Eqs. (10) and (11), Eq. (9) is rewritten as

$$\begin{aligned} &P_aS_a - P_2\left(\frac{S_b}{\left(\frac{sV_b}{\lambda K_b}+1\right)} + 2C_d\pi d_a\cos\theta_1 x_{ini}\right) - sx_{sp}\frac{S_b^2/K_b}{\left(\frac{sV_b}{\lambda K_b}+1\right)} - k_{spr}x_{sp} + 2C_d\pi d_a P_1\cos\theta_1 x_{ini} \\ &= x_{sp}\left[m_e s^2 + \left(D_f + C_d\pi d_a l\sqrt{2\rho\Delta P}\right)s + (k_{spr} + 2C_d\pi d_a P_1\cos\theta_1)\right] \end{aligned} \tag{12}$$

Considering the flow equilibrium of the PRV chamber, the equation is given as

$$K_1(P_1 - P_2) + K_{prv}x_{sp} = \frac{V_c}{\lambda}sP_2 + Q_{cl} + K_{lc}P_2 + K_b(P_2 - P_b) \tag{13}$$

where the flow pressure coefficient of pipe 1, flow gain coefficient for the PRV and leakage coefficient are denoted by K_1, K_{prv}, and K_{lc}, respectively. V_c stands for the volume of the controlled pressure chamber, and Q_{cl} represents the load flow.

Substituting Eqs. (10) and (11) into Eq. (13), the incremental equation of the PRV after some manipulations becomes,

$$(K_1P_1 - Q_{cl})\left(\frac{sV_b}{\lambda K_b}+1\right) + K_{prv}x_{sp}\left[1 + \left(\frac{V_b}{\lambda K_b} + \frac{S_b}{K_{prv}}\right)s\right] = P_2K_e\left[\left(\frac{sV_b}{\lambda K_b}+1\right)\left(\frac{sV_c}{\lambda K_e}+1\right) + \frac{V_b}{V_c}\frac{sV_c}{\lambda K_e}\right] \tag{14}$$

where $K_e = K_1 + K_{lc}$ denotes the equivalent coefficient of the flow pressure. The last term on the right of the equation is negligible by virtue of $V_b/V_c \ll 1$, and the simplified equation is expressed as

$$(K_1P_1 - Q_{cl})\left(\frac{sV_b}{\lambda K_b}+1\right) + K_{prv}x_{sp}\left[1 + \left(\frac{V_b}{\lambda K_b} + \frac{S_b}{K_{prv}}\right)s\right] = P_2K_e\left[\left(\frac{sV_b}{\lambda K_b}+1\right)\left(\frac{sV_c}{\lambda K_e}+1\right)\right] \tag{15}$$

For the discharge state, the motion of the spool is contrary to that in the filling state, and the equation is given by

$$-Q_b = K_b(P_b - P_2) = -\frac{V_b}{\lambda}sP_b + S_bsx_{sp} \tag{16}$$

Similar to the derivation for the filling state, the equation of the flow equilibrium for the PRV chamber is

$$K_b(P_b - P_2) + K_{prv}x_{sp} = \frac{V_c}{\lambda}sP_2 - Q_{cl} + K_{lc}P_2 + K_3(P_2 - P_3) \tag{17}$$

Substituting Eqs. (11) and (16) into Eq. (17) simplifies the expression to

$$(K_3P_3 + Q_{cl})\left(\frac{sV_b}{\lambda K_b} + 1\right) + K_{prv}x_{sp}\left[1 + \left(\frac{V_b}{\lambda K_b} + \frac{S_b}{K_{prv}}\right)s\right] = P_2K_e\left[\left(\frac{sV_b}{\lambda K_b} + 1\right)\left(\frac{sV_c}{\lambda K_e} + 1\right)\right] \tag{18}$$

where the flow pressure coefficient and pressure of pipe 3 are denoted by K_3 and P_3, respectively.

3.3. Clutch actuator model

The up-shifting process is mainly comprised of four phases: (I) fast filling phase (overcome resistance of clutch return spring and eliminate the gap of the friction plates when the clutch chamber is filled fast); (II) torque phase (the friction plates are compressed more and the torque is transferred from the off-going clutch to the oncoming clutch as the clutch pressure rises); (III) inertia phase (the clutch pressure increases gradually to eliminate the speed difference between the oncoming clutch and off-going clutch completely); (IV) sliding phase (the clutch pressure rises dramatically until reaching the working pressure and the clutch piston is thrust to the maximum displacement). The downshifting process is a reverse process of the upshifting process. From the above-mentioned characteristics of each phase, it is evident that the clutch pressure is a significant index of accurate control and rapid response. Hence, a dynamic model to predict the clutch pressure correctly is crucial to this study.

In reality, there is a centrifugal force acting on the clutch piston when the flow thrusts the clutch piston, which obstructs the motion of the clutch piston to a certain extent. In order to prevent the centrifugal force from affecting the clutch piston excessively, in practice, a lubricant is frequently filled into the clutch chamber. Therefore, the effect of centrifugal force is insignificant, which is ignored in modelling. The relationship among the clutch return spring, clutch pressure, and friction plates is given as

$$P_{cl}S_p - F_{rub} = m_p\ddot{x}_p + D_p\dot{x}_p + k_s(x_{s0} + x_p) \tag{19}$$

where P_{cl} is the clutch pressure, S_p denotes the cross-sectional area, D_p represents the damping coefficient. The mass and displacement of the clutch piston are denoted by m_p and x_p, respectively. The stiffness coefficient and initial compression for clutch return spring are represented by k_s and x_{s0}. Friction force F_{rub} between the rubber sealing ring and housing is expressed as

$$F_{rub} = D_aP_{cl}A_{sr} \tag{20}$$

where the damping coefficient of the rubber sealing ring and shear area of the clutch piston are denoted by D_a and A_{sr}, respectively.

Combining Eqs. (19) and (20), we obtain the motion equation of the clutch piston applied with the Laplace form as

$$P_{cl}S_p - D_aP_{cl}A_{sr} = m_ps^2x_p + D_psx_p + k_sx_p \tag{21}$$

The modelling of the clutch pressure is similar to that of the PRV according to the filling/discharge state of the fluid. Dealing with load flow Q_{cl}, the equation is written as

$$Q_{cl} = K_v(P_2 - P_{cl}) = \frac{V_{cl}}{\lambda}sP_{cl} \pm S_psx_p \tag{22}$$

where the flow pressure coefficient for damping aperture B is denoted by K_v, the volume of clutch chamber is V_{cl}. The positive sign is for the filling state and negative sign is for the discharge state.

Substituting Eqs. (19) and (21) into Eq. (22), the equation of P_{cl} can be transformed into

$$P_{cl} = \frac{K_v\lambda}{sV_{cl} + K_v\lambda}\left(P_2 \mp \frac{S_psP_{cl}(S_p - D_aA_{sr})}{K_v(m_ps^2 + D_ps + k_s)}\right) \tag{23}$$

where the negative sign denotes the filling state and positive sign denotes the discharge state.

The detailed diagram of the actuator modelling is showed in Fig. 3, and the values of the model parameters are listed in Appendix A.

4. Sensitivity analysis and Bode plots

The dynamic performance of a hydraulic system highly depends on the structure parameters; therefore, this section combines the sensitivity analysis and Bode plots to identify the key parameters for the PRV and clutch actuator.

The sensitivity analysis method mainly includes a local sensitivity analysis and global sensitivity analysis. The former is efficient in managing the simple models, whereas it probably leads to no derivatives at some points in complex models, such as discontinuous models. The latter approach determines the contribution rate of each model parameter to quantify

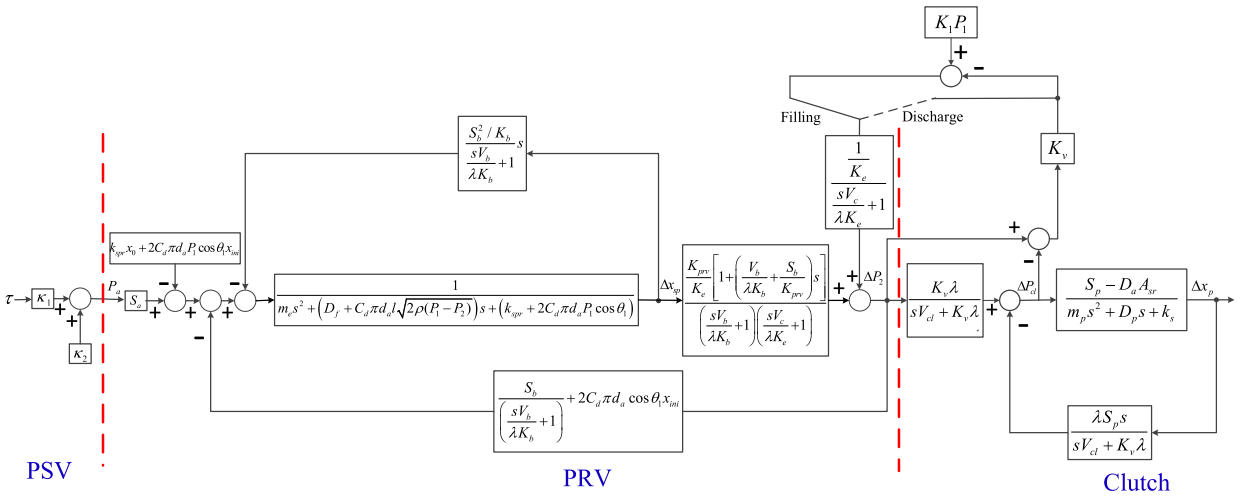

Fig. 3. The modelling diagram of the actuator.

Table 1
The range of parameter is used for sensitivity analysis.

Notation	Name	Lower limit	Upper limit
S_a	Spool area of the control side (m^2)	1.5×10^{-4}	3.8×10^{-4}
S_b	Area of the feedback side (m^2)	1×10^{-5}	7×10^{-4}
K_b	Flow pressure coefficient of feedback damping aperture A (m^3/s/Pa)	4.5×10^{-11}	8×10^{-11}
m_p	Mass of clutch piston (kg)	5	8.5
K_v	Flow pressure coefficient of the damping aperture B (m^3/s/Pa)	1×10^{-10}	5×10^{-8}
k_s	Stiffness coefficient of clutch return spring (N/m)	1×10^5	6.5×10^5
S_p	Cross-sectional area of clutch piston (m^2)	0.25	0.45

the error in the whole design space, with high computing efficiency and accuracy. Accordingly, the global sensitivity analysis is adopted based on the Monte Carlo technique.

It is vital to choose a suitable method of sampling to estimate the sensitivity. Currently, some of the prevailing methods that are used in various fields, such as, random sample, Markov Chain Monte Carlo method, importance sample, and Latin hypercube sample (LHS). Since the LHS can ensure that the real variability of the sampling number is representative, it is widely employed to construct simulation variables. This study similarly assumes that all the parameters are independent; moreover, the distributions of K_v, S_p, k_s, and K_b are considered to be uniform and those of others are normal. The design parameters are listed in Table 1. Applying the LHS to sample the random set, 70 samples are chosen to estimate the sensitivity. The global sensitivity results for the parameters are shown in Fig. 5.

Bode plots are often used to describe the frequency response, which can also analyse the influence of the parameter to a certain extent. Here, defining the working frequency as 5 rad/s based on the actual situation, the equation assessment of parameter is given as follows:

$$\sigma = \frac{\varphi_{\max} - \varphi_{\min}}{\varphi_{\max}} \tag{24}$$

where σ denotes the Bode plot index, $\varphi_{\max}$ is the phase of the maximum boundary and $\varphi_{\min}$ is the phase of the minimum boundary in the Bode plot. Fig. 4 shows the relationships of the main influence factors versus frequency. Based on the plots, the assessment of all the parameters is shown in Fig. 5.

As shown in Fig. 5, although the Bode plot index of the stiffness coefficient of the clutch return spring k_s is much higher than the ones assessed by the global sensitivity method, the other parameters are close to the results of the sensitivity analysis. Furthermore, the assessment results of the global sensitivity index and Bode plot index have the same trend; specifically, the estimations applied by the two methods for the influence of the structure parameters are similar. Therefore, the Bode plots are effective for evaluating the key parameters in the system.

It also can be seen that the flow pressure coefficient of the aperture K_v is the most influencing factor among the selected parameters. In fact, the parameter design of the throttle played a prominent role in [21,22]. If the throttle coefficient is extremely small, the flow rate increases less resulting in prolonging the shifting time. Conversely, if it is extremely large, it may cause the fluid pressure to overshoot or the clutch pressure to fluctuate considerably, even inducing the self-excited vibration effect. Stiffness coefficient k_s is the second most critical factor in both the estimation methods. Generally, the space of the clutch chamber is restricted; thus, a large spring stiffness is often chosen. However, an extremely large spring stiffness also influences the response of the clutch pressure. Hence, the selection of the spring stiffness should also be paid

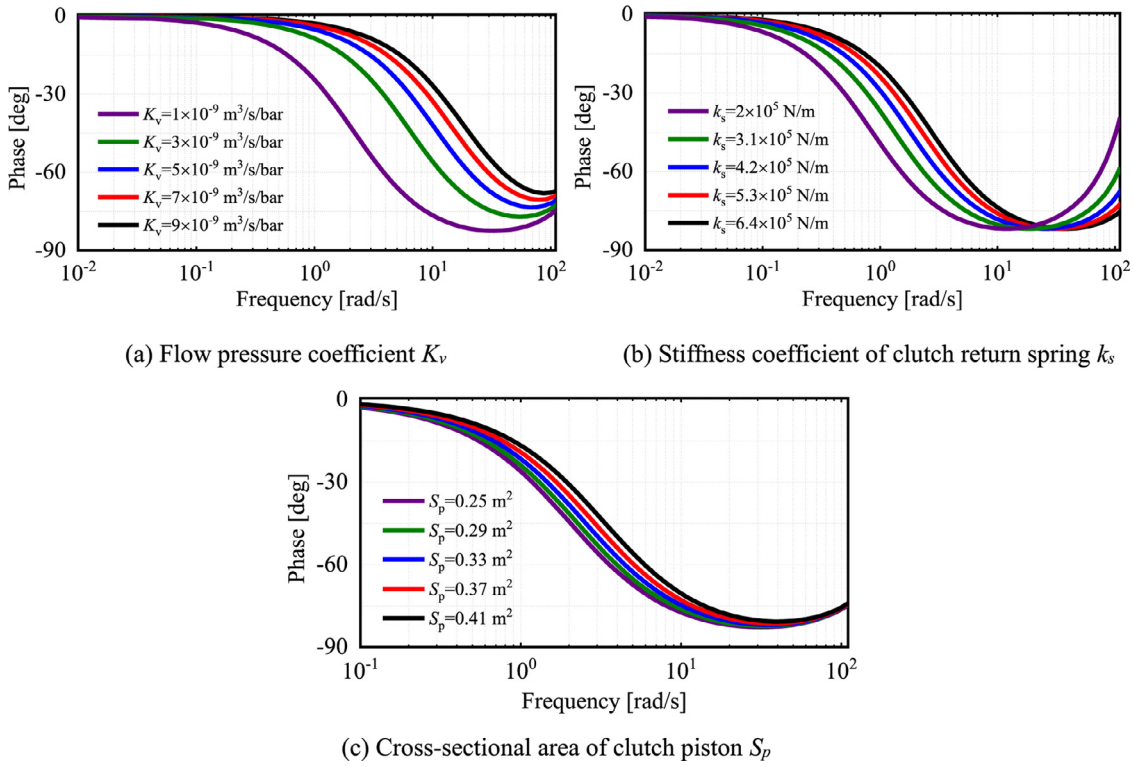

(a) Flow pressure coefficient K_v

(b) Stiffness coefficient of clutch return spring k_s

(c) Cross-sectional area of clutch piston S_p

Fig. 4. The phase of Bode Plots for main parameters.

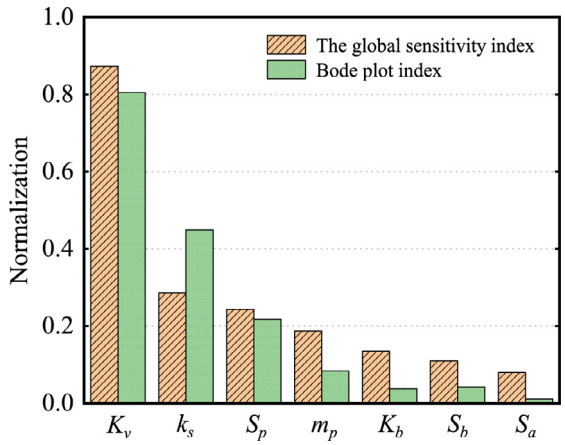

Fig. 5. Comparison of sensitivity analysis and Bode plots index after normalization.

significant attention. In view of the Bode plot index, because the area of the pilot chamber S_a is sufficiently small, we select six design parameters to perform the optimization, which is described in the next section, except for S_a.

5. Optimal design

Section 4 analyses the influence to the system for each of parameter. Considering the efficiency of optimization, six structure parameters, K_v, k_s, S_p, m_p, S_b, and K_b, are picked up to optimize.

5.1. Optimization model

To improve the comfort of shifting, the clutches should be engaged/separated synchronously, implies that the clutch pressure should be controlled precisely and the response should be maximally rapid. In general, a high flow rate can speed

up response time, but the accompanying phenomenon of overcharging leads to the severe vibration of the system. If the vibration is severe, the clutches may be engaged/separated inaccurately, causing discomfort to the passengers. In terms of a low flow rate, it only causes a slight vibration, but with a delay in the time of response for shifting process causes a dramatic increase in the fuel consumption. Therefore, to adjust the inconsistency between the time of response and vibration caused by overcharging, an optimal scheme is established based on the analysis results presented in Section 4. The objective function is written as

$$\mathrm{Min}J = \frac{1}{N}\sum_{i=1}^{N}|P_{cl}(t) - P_{ideal}(t)| \tag{25}$$

where P_{ideal} is the ideal clutch pressure. t is the time of simulation from 0 to 6 s. N denotes the number of points that are calculated during 0–6 s.

The constraint conditions for the structure parameters are described as below.

On account of the natural frequency of the system, $(k_s/m_p)^{1/2}$ should be satisfied with the ranging from 30–55 Hz which can be expressed as (26-a)

$$30 \le \sqrt{k_s/m_p} \le 55 \tag{26-a}$$

The pump flow Q_{pump} in a heavy-duty vehicle is approximately 100 L/min. In general, the maximum flow in the valve should be higher than the pump flow [11]. Furthermore, the flow in the valve should be restricted in a reasonable range considering the flow saturation. Therefore, the limitations for K_v and K_b are expressed as (26-b) and (26-c)

$$K_v > \frac{Q_{pump}}{10^6} \tag{26-b}$$

$$\frac{K_v}{K_b} < \frac{Q_{cl\max}(P_2 - P_b)}{Q_{b\max}(P_2 - P_{cl})} + K_{lc} \tag{26-c}$$

In practice, the diameter of the feedback chamber should be less than that of the PRV chamber but it should be larger than 2/3rd of the valve diameter. This restriction is expressed in (26-d)

$$\frac{2}{3}\pi d_a^2 < S_b < \pi d_{prv}^2 \tag{26-d}$$

where d_{prv} denotes the diameter of the PRV chamber.

In consideration of the length of the clutch chamber and response time of the clutch, S_p should satisfy (26-e)

$$\frac{k_s x_{s0}}{P_{cl}} < S_p < \frac{k_s(x_{p\max} + x_{s0}) + D_a P_{cl} A_{sr}}{P_{cl}} \tag{26-e}$$

To achieve the requirement of a rapid response, the clutch pressure should reach 8 bar at least when the time is 1.8 s, which is written as

$$P_{cl}(1.8) \ge 8\mathrm{bar} \tag{26-f}$$

In summary, the optimization problem can be expressed as

$$\begin{cases} \textbf{Find}\ \text{Eq. (25)}; \\ \textbf{Design variables}\ [k_s, m_p, K_v, K_b, S_p, S_b]; \\ \textbf{Subjected to}\ \text{Eqs. } (26-a) \text{ to } (26-f). \end{cases} \tag{27}$$

5.2. Artificial bee colony algorithm

The ABC algorithm is a methodology imitating the behaviours of bees seeking honey to deal with the optimization problem. It is comprised of four elements: food source, employed bees, onlooker bees and scout bees. The food source stands for the solution of the problem. In order to find a better food source, the employed bees search and memorize the information of the food source. Concurrently, they share their memory with the onlooker bees at a certain probability. According to the memory, the onlooker bees prefer to select a better food source, i.e., select a better solution. The employed bees who cannot search for a better food source at within a specific number of trials will become scout bees to find another food source via stochastic search method and abandon the previous food source [40].

Based on the principle of ABC algorithm, the steps are organized as follows.

Step 1: Initialize the number of bees *NB*, onlooker bees number *N_onlooker*, the number of variable *Nvar*, the lower and upper restrictions of variables *lb* and *ub*, the number of food source *SN*, the maximum cycle *MCN*, the number of solution failing to improve *Limit*, the number of trials before abandon previous solution *Trail*.

Step 2: Generate the initial solutions U_{iter} in the specific range and calculate the objective function J_{iter}.

Step 3 (employed bees): Generate new solutions and compare with the initial solutions. Calculate the objective function J_i for new solutions. Update the solutions if $J_i < J_{iter}$.

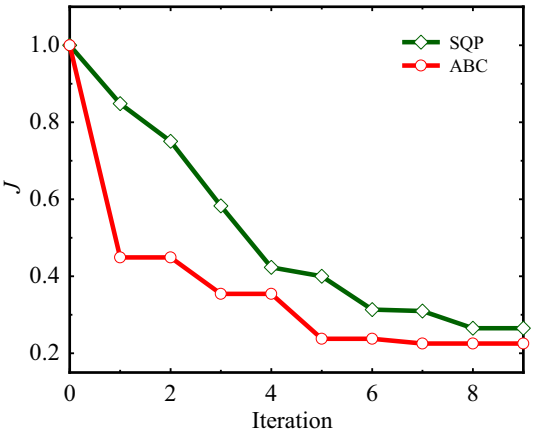

Fig. 6. The objective function for each of iteration.

Table 2
The comparison of ABC and SQP after optimization.

Algorithm	K_v	k_s	S_p	m_p	K_b	S_b	J	Time (min)
ABC	8.074×10^{-9}	2.325×10^{5}	0.325	7.365	7.115×10^{-11}	2.021×10^{-4}	0.226	135.943
SQP	7.326×10^{-9}	2.000×10^{5}	0.325	7.500	6.374×10^{-11}	2.045×10^{-4}	0.265	153.710

Step 4 (onlooker bees): Calculate the fitness based on the Eq. (28)

$$fitness(x_i) = \begin{cases} \dfrac{1}{1+x_i}, & x_i \geq 0 \\ 1+|x_i|, & x_i < 0 \end{cases} \tag{28}$$

The probability of fitness is calculated based on Eq. (29), and the solution is selected based on P_i

$$P_i = \frac{fitness(J_i)}{\sum_{n=1}^{SN} fitness(J_n)} \tag{29}$$

New solutions are generated and compared with the initial solutions. The objective function J_n is calculated for the new solutions. The solutions are updated if $J_n < J_{iter}$.

Step 5 (scout bees): The solutions is reinitialized if $Trail > Limit$.

Step 6: The values of the best solution and objective function are stored.

The pseudo code is presented in Appendix B.

5.3. Optimization results

In this section, the proposed model is redesigned by the SQP and ABC algorithms, respectively. The initial conditions are set as follows: The pulse signals are transmitted by the PSV at 24 V. The pressure of supply fluid is 10 bar, and the initial compression of the clutch return spring is 0.5 mm. For the ABC algorithm, the number of bees is 50, onlooker bees number is 25, number of food source is 25, maximum cycle is 50, and number of solutions failing to improve is 15.

The ABC algorithm and SQP are coded in MATLAB R2016a and run by dual-core parallel computation with Intel i5-7400 @ 3.00 GHz. The optimization results are provided in Fig. 6 and Table 2. Less iterations are required for the objective function to reach a constant value by the ABC algorithm than with the SQP method. It takes approximately 136 min for the ABC algorithm to converge, and the SQP method consumes approximately 154 min. In terms of the optimization effect, the smaller the objective function J, the closer the simulation profile is to the reference profile, as illustrated in Fig. 7. For the ABC algorithm, the value of J is 0.226 and for the SQP method is 0.265. This demonstrates that the optimization with ABC algorithm is closer to the reference profile than with the SQP method, indicating a better optimization effect. In summary, the ABC algorithm is well suitable to optimize this model. The structure parameters change during each iteration in the ABC algorithm, as presented in Appendix C. K_v, S_p, m_p, and S_b increase whereas k_s, K_b decrease after the optimization. The detailed reasons for the variation in the parameters are given in Section 6.

6. Optimization results and discussions

To demonstrate the variation in the shifting performance of the original design and optimized design intuitively, the optimized profiles of the clutch pressure, response time, flow rate, jerk, acceleration of the clutch piston, steady flow force,

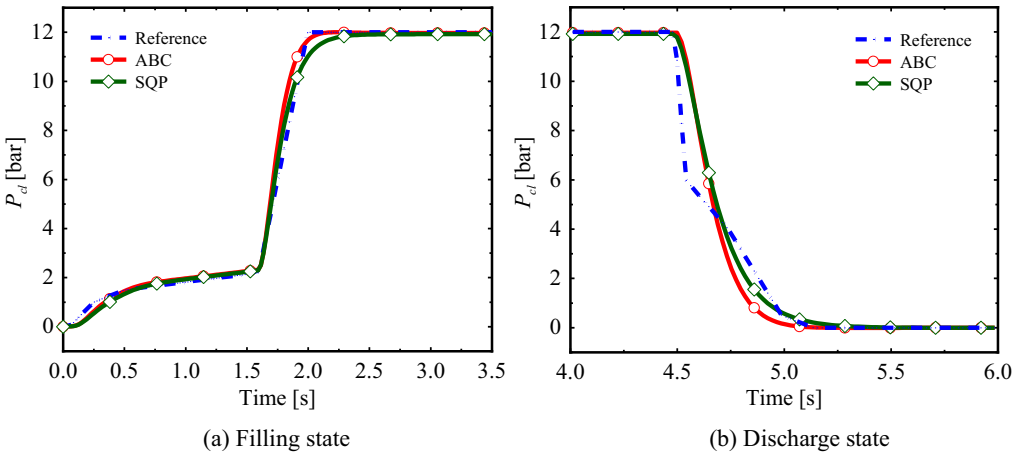

Fig. 7. The comparison of clutch pressure obtains by different algorithm.

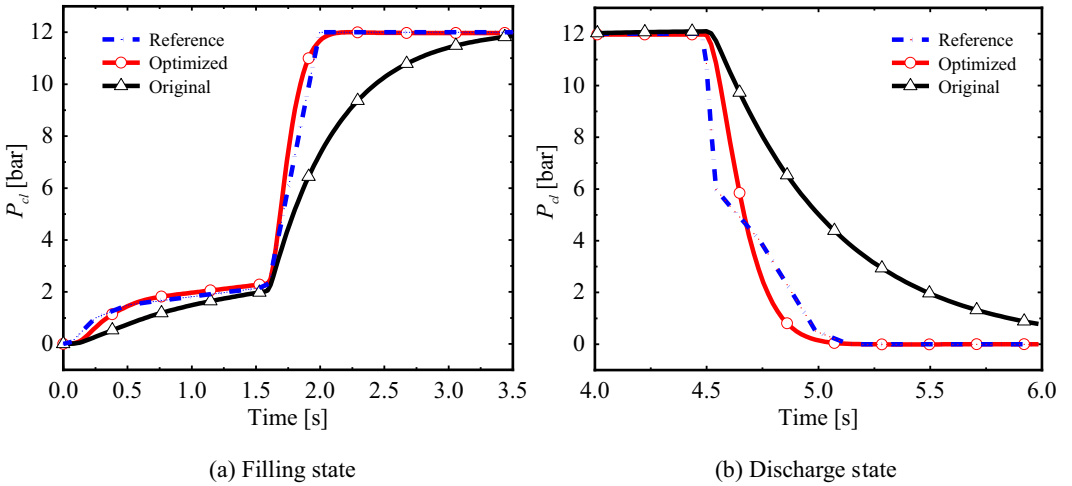

Fig. 8. The comparison of clutch pressure. (For interpretation of the references to color in this figure, the reader is referred to the web version of this article.)

and fluid temperature rise will be compared with those of the original profiles. Additionally, the detailed discussions are also given in this section.

6.1. Clutch pressure

As depicted in Fig. 8, the blue line denotes the reference clutch pressure regarded as the most ideal situation of a smooth shift for a heavy-duty vehicle. The black line and red line represent the original and optimized profiles, respectively.

For the fast filling phase (0–0.25 s) in the filling state shown in Fig. 8(a), the optimized profile is much closer to the reference profile owing to oil flow increase in pipe 1. Moreover, it only takes approximately 2.05 s for the optimized profile to end the shifting process, whereas the same process for the original profile demands approximately 3.4 s, which makes the shifting rough. For the discharge state shown in Fig. 8(b), it is notable that the optimized profile approaches the reference profile for any phase. Considering the aspects of the shifting performance, it is a reasonable scheme for the response time of the optimized profile to approach the ideal situation at the expense of appropriate overcharging. For the optimized design, the shifting process is shortened by 1.35 s and the deviation of the clutch pressure from reference pressure is no more than 1 bar in the filling state. Thus it can be inferred that the performance of the shifting is improved after optimization.

As a supplement of Fig. 8, Fig. 9 gives the deviation of the response time intuitively. In Fig. 9(a), the blue dot line stands for the standard line and the optimization goal is to make the black line maximally close to the standard line. The closer the line approaches the standard, the more accurate the shifting control will be. It is clear that the optimized design (red line) is closer to the standard line than the original (black line), indicating the performance of shifting can be controlled more precise. The end time for each phase during the shifting is shown in Fig. 9(b), where t_1, t_2, and t_3 denote the end time of the fast filling phase, torque phase, and inertia phase in the filling state, respectively. t_4, t_5, and t_6 denote the end time of

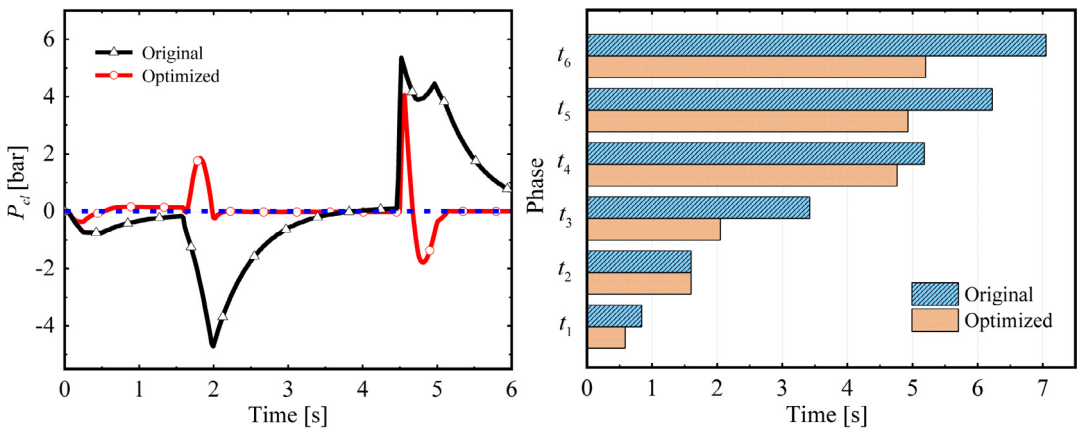

(a) The deviation for each time step (b) The comparison of end time for each phase

Fig. 9. The response time for shifting. (For interpretation of the references to color in this figure, the reader is referred to the web version of this article.)

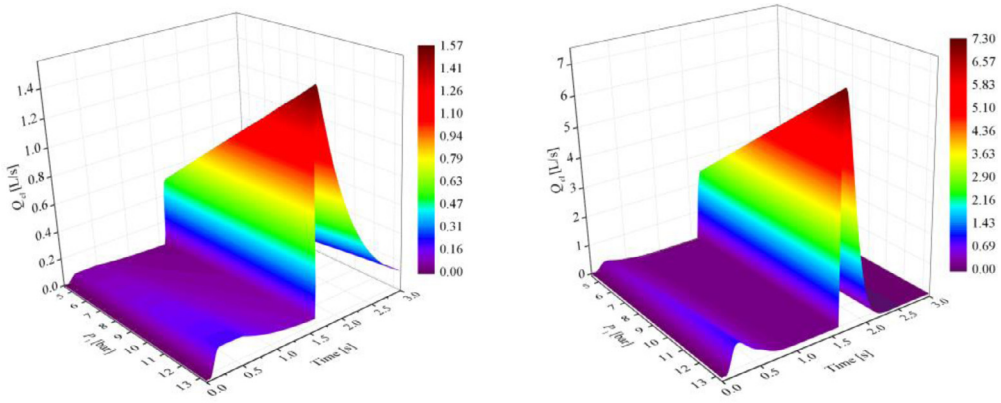

(a) Original (b) Optimized

Fig. 10. The flow rate at different supply pressure.

the fast filling phase, torque phase and inertia phase in the discharge state, respectively. It can be seen that the response time is much shorter for the optimized design.

6.2. Flow rate

The relationship between supply pressure P_1, flow rate Q_{cl}, and filling time t is presented in Fig. 10. P_1 varies linearly with Q_{cl} because the effect of pump and pipe is not considered in the model. Under the condition of 10 bar supply pressure, on the basis of the integral of Q_{cl} to t, the average flow for original design is only 0.67 L/s, whereas it is run up to 1.49 L/s for the optimized design owing to the increase in K_v, corresponding to 3.4 s and 2.05 s of the shifting time, respectively. Based on the simulation results, it can be interpreted that the flow rate influences the response time significantly, which verifies that K_v is the most crucial structure parameter amongst the selected parameters. In practice, a higher flow often has an advantage of accelerating the response speed for the heavy-duty vehicles.

6.3. Jerk and acceleration

To estimate the performance of shifting, jerk J_e, the rate of change for the vehicle longitudinal acceleration, is introduced in this section. It can be calculated by $J_e = r_w / (i_0 \times I_w) \times dT_{out} / dt$, where r_w is the dynamic radius for the wheel, i_0 is the transmission ratio of the driving axle, I_w is the equivalent moment of inertia in the longitudinal direction of the vehicle, and T_{out} is the output torque of the transmission. The index excludes the influence of the jolt caused by the road surface and reflects the subjective feelings of the passengers toward drive comfort.

Fig. 11 shows the difference in the jerk of the original parameters and optimized parameters. It is evident that the jerk of the optimized design is larger than that of the original design. The reason is that this optimization enlarges K_v to

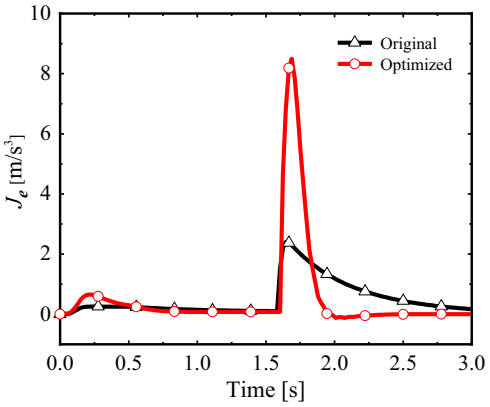

Fig. 11. The comparison of jerk.

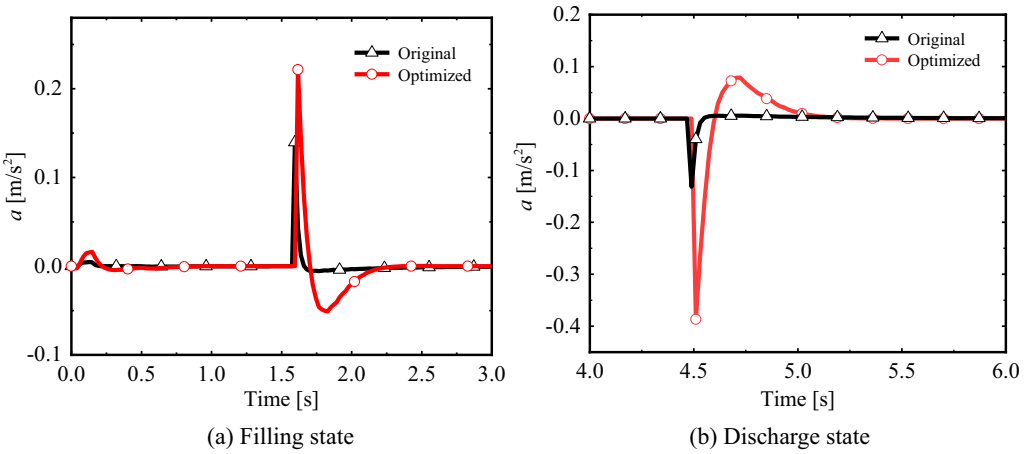

Fig. 12. The comparison of acceleration of clutch piston.

accommodate more fluid to flow into the clutch chamber simultaneously to accelerate the response time for obtaining a better shifting performance overall. Generally, the maximum jerk for most vehicles should fall within a certain range; for instance, the recommendation in Germany is that it should not exceed 10 m/s^3 [41]. Although the optimized jerk increases with the flow, it is still within the advisable range. For the original jerk, it is actually sufficiently small, however, the shifting time delay is extremely large, leading to an insufficient power output and increase in the clutch wear.

The acceleration of the clutch piston is illustrated in Fig. 12. It can be seen that the optimized clutch acceleration is higher than the original irrespective of the phase. It should be noted that the hysteresis delays the motion of the clutch piston occurring when the flow is high, e.g., at 1.6 s in the filling state and 4.5 s in the discharge state. Despite the high flow with the hysteresis, the motion of the clutch piston is faster and the overall response time is shorter than those of the original low flow.

6.4. Steady flow force

In a high flow circumstance, the hysteresis affected by the flow force will enlarge, as illustrated in Fig. 12. Consequently, considering the flow force for the model of the actuator in heavy-duty vehicles is necessary. The detailed flow distribution in the PRV calculated by COMSOL Multiphysics is shown in Fig. 13. For the optimized design, the flow increases significantly and the maximum velocity of flow in pipe 2 can reach to nearly 23 m/s, whereas it only reaches to approximately 8 m/s for original design. With the flow increase, discharge coefficient C_d increases and jet angle θ_1 slightly decreases. The explicit change of C_d and θ_1 is shown in Fig. 14 via curve fitting for different pipe openings. Here, x_{vo} is the opening of pipe 1. According to the variation in C_d and θ_1, the steady flow force is shown in Fig. 15. The value of the transient flow force is extremely small in comparison with pilot force F_a; therefore, we only present the steady flow force. Compared to the

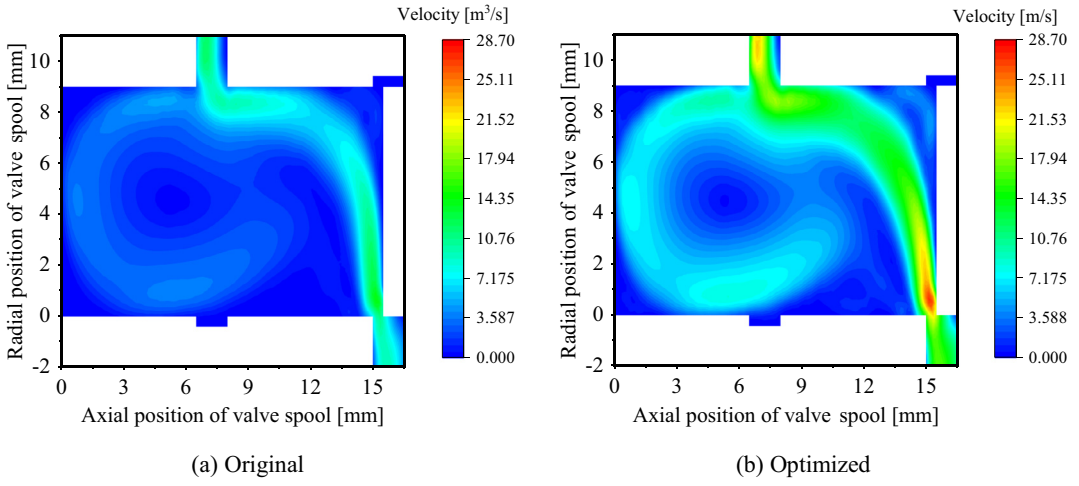

Fig. 13. The comparison of flow distribution.

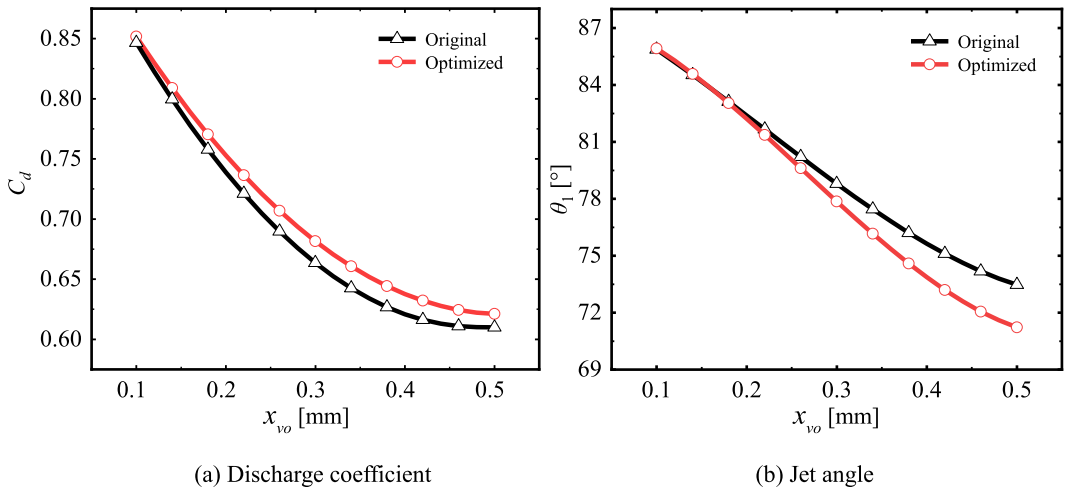

Fig. 14. The comparison of discharge coefficient and jet angle.

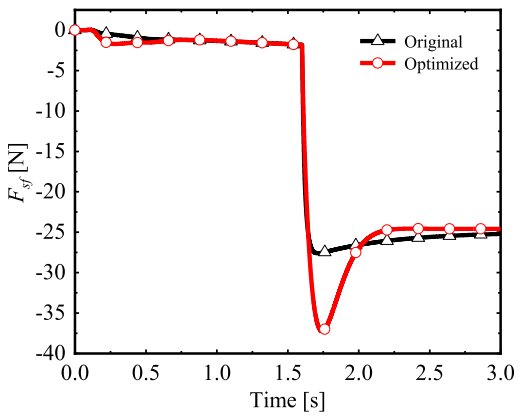

Fig. 15. The steady flow force in filling state.

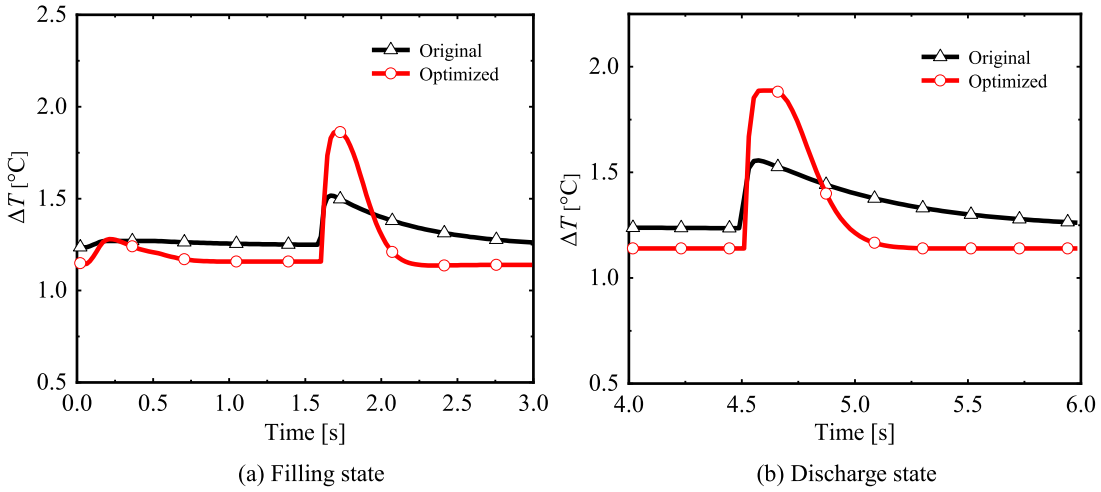

Fig. 16. The comparison of temperature rise of clutch fluid.

original design, there is no significant change in the steady flow force of the optimized design. Specifically, the force does not give rise to a significant delay in the response before and after the optimization.

6.5. Temperature rise

The system is assumed to be in an isolated environment. Fig. 16 shows the comparison of the temperature rise of the clutch oil for the original and optimized profiles. Clearly, maximum temperature rise does not exceed 2 °C under both the original and optimized conditions. Therefore, it can be deduced that the temperature rise of the clutch oil has no significant effect on the system performance, which can be ignored in the modelling.

7. Conclusions

In this study, an accurate model has been established to reflect the real shifting process for an electro-hydraulic actuator. Moreover, the key parameters of the model are identified by means of Bode plots and the results are validated by sensitivity analysis. According to the rankings of the influential parameters, ABC algorithm and SQP method are employed to optimize the model, respectively. The significant conclusions are obtained as follows:

(1) The key parameters identified by sensitivity analysis and Bode plots obtain the same ranking. Therefore, for identifying design variables, the sensitivity analysis may be replaced by using Bode plots.
(2) K_v is the most critical parameter with regard to the response time.
(3) Compared with the SQP method, the ABC algorithm is more efficient and better to figure out the optimal parameters for the proposed model.
(4) For the optimized design, the average flow rate reaches to 1.49 L/s leading to a significant increase in acceleration of clutch piston, which shortens the time response 1.35 s than the original design.
(5) There is little change for the steady flow force before and after optimization so it doesn't bring about the significant effect on the response time.
(6) The temperature rise is no more than 2 °C irrespective of the design parameters change. Hence, the change of the fluid temperature can be neglected.

Declaration of Competing Interest

None

Funding

This work was supported by the National Natural Science Foundation of China [grant numbers 2018NSFC51805100]; the China Postdoctoral Science Foundation funded project [grant numbers 2019T120374]; the Guangxi Natural Science Foundation Program [grant number 2017GXNSFBA198198].

Appendix A

Table A1
Parameters of electro-hydraulic actuator.

Symbol	Description	Value
m_e	Equivalent mass of spool	6.5×10^{-3} (kg)
K_1	The flow pressure coefficient of pipe 1	7.57×10^{-11} (m^3/s/Pa)
K_{prv}	Flow gain coefficient of the PRV	5.35 (m^3/s/Pa)
K_{lc}	Leakage coefficient	2.26×10^{-9} (m^3/s/Pa)
V_b	Volume of feedback chamber	7.51×10^{-8} (m^3)
V_c	Volume of controlled pressure chamber	3×10^{-5} (m^3)
k_{spr}	Spring coefficient of PRV	1061 (N/m)
x_0	Initial displacement of spring	10^{-4} (m)
c_v	The coefficient of flow velocity	0.98
P_1	The pressure of pipe 1	1×10^6 (Pa)
D_f	Viscous damping constant	5930 (N/m/s)
l	Length of PRV chamber	0.1 (m)
d_a	Diameter of valve	9×10^{-3} (m)
x_{ini}	The overlap of pipe 1 at the initial position	0.1×10^{-3} (m)
α_o	Overlap of spool	1.2×10^{-3} (m)
x_{s0}	Initial compression of clutch return spring	5×10^{-3} (m)
V_{cl}	Volume of clutch chamber	3.84×10^{-4} (m^3)
D_p	Damping coefficient	1186 (N/m/s)
ρ	Density of hydraulic fluid	880 (kg/m^3)
λ	Effective bulk modulus of hydraulic fluid	1.7×10^9 (Pa)
r_w	The dynamic radius for the wheel	0.55 (m)
i_0	The transmission ratio of drive axle	15.53
I_w	The equivalent moment of inertia in longitudinal direction of the vehicle	15 (kg·m^2)

Appendix B

Algorithm 1
Pseudo code of ABC algorithm.

Initialize Nvar, lb, ub, NB, SN, N_onlooker, MCN, Limit, Trial.
for iteration = 1 to SN **do**
  Initialize the solutions $U_{iter} = U_{lb} + \lambda(U_{ub} - U_{lb})$.
  λ is uniformly distributed in [0,1]. U_{ub} and U_{lb} are the upper and lower limit of U_{iter}, respectively.
  Calculate the objective function J_{iter} for each U_{iter}.
end for
for cycle = 1 to MCN **do**
  for i = =1 to SN **do**
    Generate an arbitrarily value k from the integers 1 to SN and k ≠ i.
    Generate new solutions $Z_i = U_i + \alpha(U_i - U_k)$, where α is uniformly distributed number in [−1,1].
    Calculate the objective function J_i of each Z_i.
    New solutions $Z_i \in$ [lb,ub].
  if $J_i < J_{iter}$ **then**
    Update the value of objective function and the solutions.
    Trial(j) ← 0 otherwise Trial(j) ← Trial(j) + 1.
  end if
  end for
    Calculate the fitness(U) by Eq. (28) and the probability of fitness P_i by Eq. (29).
    Select the solutions by roulette wheel according to the probability of fitness.
    for n = =1 to N_onlooker **do**
      Generate an arbitrarily value p from the integers 1 to SN and p ≠ n.
      Generate new solutions $Z_n = U_n + \alpha(U_n - U_p)$, $\alpha \in [-1,1]$, $Z_n \in$ [lb,ub]
      Calculate the objective function J_n for each Z_n.
    if $J_i < J_{iter}$ **then**
      Update the value of objective function and the solutions.
      Trial(j) ← 0 otherwise Trial(j) ← Trial(j) + 1.
    end if

(*continued on next page*)

Algorithm 1 (*continued*)

```
            end for
        for each U_iter do
            if Trial(i) > Limit then
                Reinitialize U_i and Trial(i) ← 0.
            end if
        end for
    end for
    Memorize the best solution and objective function.
```

Appendix C

Table A2
The value of parameters and objective function for iteration procedure.

Iteration	K_v (m^3/s/Pa)	k_s (N/m)	S_p (m^2)	m_p (kg)	K_b (m^3/s/Pa)	S_b (m^2)	J
0	1.170×10^{-9}	4.000×10^{5}	0.300	6.150	6.861×10^{-11}	1.930×10^{-4}	1.000
1	2.602×10^{-9}	3.993×10^{5}	0.322	7.068	6.547×10^{-11}	2.034×10^{-4}	4.489×10^{-1}
2	2.602×10^{-9}	3.993×10^{5}	0.322	7.068	6.547×10^{-11}	2.034×10^{-4}	4.489×10^{-1}
3	2.602×10^{-9}	4.854×10^{5}	0.322	7.068	6.547×10^{-11}	2.034×10^{-4}	3.543×10^{-1}
4	2.602×10^{-9}	4.854×10^{5}	0.322	7.068	6.570×10^{-11}	2.034×10^{-4}	3.541×10^{-1}
5	8.074×10^{-9}	2.325×10^{5}	0.313	7.015	7.115×10^{-11}	2.015×10^{-4}	2.374×10^{-1}
6	8.074×10^{-9}	2.325×10^{5}	0.313	7.015	7.115×10^{-11}	2.015×10^{-4}	2.374×10^{-1}
7	8.074×10^{-9}	2.325×10^{5}	0.325	7.015	7.115×10^{-11}	2.015×10^{-4}	2.255×10^{-1}
8	8.074×10^{-9}	2.325×10^{5}	0.325	7.105	7.115×10^{-11}	2.015×10^{-4}	2.255×10^{-1}
9	8.074×10^{-9}	2.325×10^{5}	0.325	7.365	7.115×10^{-11}	2.021×10^{-4}	2.255×10^{-1}

References

[1] X.Y. Song, M.Z. Zulkefli, Z.X. Sun, H.C. Miao, Automotive transmission clutch fill control using a customized dynamic programming method, J. Dyn. Syst. Meas. Control Trans. ASME 133 (2011) 054503.
[2] F. Chiara, M. Canova, A review of energy consumption, management, and recovery in automotive systems, with considerations of future trends, Proc. Inst. Mech. Eng. Part D J. Automob. Eng. 227 (2013) 914–936.
[3] J.X. Liu, L.D. Yu, Q.L. Zeng, Q.Y. Li, Synthesis of multi-row and multi-speed planetary gear mechanism for automatic transmission, Mech. Mach. Theory 128 (2018) 616–627.
[4] D. Kim, H. Peng, S. Bai, J.M. Maguire, Control of integrated powertrain with electronic throttle and automatic transmission, IEEE Trans. Control Syst. Technol. 15 (2007) 474–482.
[5] F.Z. Ji, Y.P. Bao, Y. Zhou, et al., Investigation on performance and implementation of tesla turbine in engine waste heat recovery, Energy Convers. Manage. 179 (2019) 326–338.
[6] S.C. Lee, Y. Zhang, D.H. Jung, B.C. Lee, A systematic approach for dynamic analysis of vehicles with eight or more speed automatic transmission, J. Dyn. Syst. Meas. Control Trans. ASME 136 (2014) 051008.
[7] P.K. Wong, Z.C. Xie, Y.Q. Chen, L.M. Tam, Development of a novel dual-belt van doorne's continuously variable transmission for automobiles - a preliminary study, Int. J. Struct. Stab. Dyn. 18 (2018) 1850016.
[8] P. Setlur, J.R. Wagner, D.M. Dawson, B. Samuels, Nonlinear control of a continuously variable transmission (CVT), IEEE Trans. Control Syst. Technol. 11 (2003) 101–108.
[9] X.Y. Xu, Y.H. Liang, M. Jordan, P. Tenberge, P. Dong, Optimized control of engine start assisted by the disconnect clutch in a P2 hybrid automatic transmission, Mech. Syst. Signal Process. 124 (2019) 313–329.
[10] F. Meng, G. Tao, T. Zhang, Y.H. Hu, P. Geng, Optimal shifting control strategy in inertia phase of an automatic transmission for automotive applications, Mech. Syst. Signal Process. 60-61 (2015) 742–752.
[11] Y. Wang, S.R. Guo, H.K. Dong, Modeling and control of a novel electro-hydrostatic actuator with adaptive pump displacement, Chin. J. Aeronaut. (2018) In press, doi:10.1016/j.cja.2018.05.020.
[12] F. Meng, G. Tao, H.Y. Chen, Smooth shift control of an automatic transmission for heavy-duty vehicles, Neurocomputing 159 (2015) 197–206.
[13] S.H. Wang, Y.J. Liu, Z. Wang, et al., Adaptive fuzzy iterative control strategy for the wet-clutch filling of automatic transmission, Mech. Syst. Signal Process. 130 (2019) 164–182.
[14] F. Meng, H. Zhang, D.P. Cao, H.Y. Chen, System modeling, coupling analysis, and experimental validation of a proportional pressure valve with pulsewidth modulation control, IEEE/ASME Trans. Mechatron. 21 (2016) 1742–1753.
[15] S.K. Chung, C.R. Koch, A.F. Lynch, Flatness-based feedback control of an automotive solenoid valve, IEEE Trans. Control Syst. Technol. 15 (2007) 394–401.
[16] H.C. Jian, W. Wei, H.C. Li, Q.D. Yan, Optimization of a pressure control valve for high power automatic transmission considering stability, Mech. Syst. Signal Process. 101 (2018) 182–196.
[17] Z.P. Xu, X.Y. Wang, Development of a novel high pressure electronic pneumatic pressure reducing valve, J. Dyn. Syst. Meas. Control 133 (2011) 011011.
[18] B. Xu, R.Q. Ding, J.H. Zhang, Q. Su, Modeling and dynamic characteristics analysis on a three-stage fast-response and large-flow directional valve, Energy Convers. Manag. 79 (2014) 187–199.
[19] Q.P. Chen, H. Ji, Y. Zhu, X.B. Yang, Proposal for optimization of spool valve flow force based on the matlab-amesim-fluent joint simulation method, IEEE Access 6 (2018) 33148–33158.
[20] Z.J. Jin, L. Wei, L.L. Chen, J.Y. Qian, M. Zhang, Numerical simulation and structure improvement of double throttling in a high parameter pressure reducing valve, J. Zhejiang Univ. Sci. A 14 (2013) 137–146.
[21] X.F. He, D.X. Zhao, X. Sun, B.H. Zhu, Theoretical and experimental research on a three-way water hydraulic pressure reducing valve, J. Pressure Vessel Technol. 139 (2017) 041601.
[22] O. Gad, Modeling and simulation of the steady-state and transient performance of a three-way pressure reducing valve, J. Dyn. Syst. Meas. Control Trans. ASME 138 (2016) 031001.

[23] P. Athanasatos, T. Costopoulos, Proactive fault finding in a 4/3-way direction control valve of a high pressure hydraulic system using the bond graph method with digital simulation, Mech. Mach. Theory 50 (2012) 64–89.
[24] C. Mizrak, I. Esen, The optimisation of rail vehicle bogie parameters with the fuzzy logic method in order to improve passenger comfort during passage over bridges, Int. J. Heavy Veh. Syst. 24 (2017) 113–139.
[25] H. Hamdad, C. Pézerat, B. Gauvreau, C. Locqueteau, Y. Denoual, Sensitivity analysis and propagation of uncertainty for the simulation of vehicle pass-by noise, Appl. Acoust. 149 (2019) 85–98.
[26] W.L. Chen, X.M. Zhang, H. Li, J.Y. Wei, S. Fatikow, Nonlinear analysis and optimal design of a novel piezoelectric-driven compliant microgripper, Mech. Mach. Theory 118 (2017) 32–52.
[27] S.J. Kim, C.H. Kim, S.Y. Jung, Y.J. Kim, Optimal design of novel pole piece for power density improvement of magnetic gear using polynomial regression analysis, IEEE Trans. Energy Convers. 30 (2015) 1171–1179.
[28] R. Bahloul, H. Arfa, H. Belhadjsalah, A study on optimal design of process parameters in single point incremental forming of sheet metal by combining box-behnken design of experiments, response surface methods and genetic algorithms, Int. J. Adv. Manuf. Technol. 74 (2014) 163–185.
[29] S. Prabhu, M. Uma, B.K. Vinayagam, Surface roughness prediction using Taguchi-fuzzy logic-neural network analysis for CNT nanofluids based grinding process, Neural Comput. Appl. 26 (2014) 41–55.
[30] A. Haj-Fraj, F. Pfeiffer, A model based approach for the optimization of gearshifting in automatic transmissions, Int. J. Veh. Des. 28 (2002) 171–188.
[31] F. Meng, P. Shi, H.R. Karimi, H. Zhang, Optimal design of an electro-hydraulic valve for heavy-duty vehicle clutch actuator with certain constraints, Mech. Syst. Signal Process. 68-69 (2016) 491–503.
[32] R. Amirante, L.A. Catalano, C. Poloni, P. Tamburrano, Fluid-dynamic design optimization of hydraulic proportional directional valves, Eng. Optim. 46 (2014) 1295–1314.
[33] H.C. Jian, W. Wei, H.C. Li, Q.D. Yan, Optimization of a pressure control valve for high power automatic transmission considering stability, Mech. Syst. Sig. Process. 101 (2018) 182–196.
[34] D. Karaboga. An idea based on honey bee swarm for numerical optimization, Technical report-tr06. Turkey: Erciyes university, engineering faculty, computer engineering department 2005.
[35] D.L. Yang, Y.L. Liu, S.B. Li, X.J. Li, L.Y. Ma, Gear fault diagnosisbasedon supportvectormachine optimized by artificial bee colony algorithm, Mech. Mach. Theory 90 (2015) 219–229.
[36] V. Baradaran, A Shafaei, ah Hosseinian. stochastic vehicle routing problem with heterogeneous vehicles and multiple prioritized time windows: Mathematical modeling and solution approach, Comput. Ind. Eng. 131 (2019) 187–199.
[37] K. Li, Y.Y. Yu, Y.L. Wang, Z.W. Hu, Research on structural optimization method of FRP fishing vessel based on artificial bee colony algorithm, Adv. Eng. Softw. 121 (2018) 250–261.
[38] F. Meng, H.Y. Chen, T. Zhang, X.Y. Zhu, Clutch fill control of an automatic transmission for the heavy-duty vehicle applications, Mech. Syst. Sig. Process. 64-65 (2015) 16–28.
[39] A.E. Balau, C.F. Caruntu, C. Lazar, Simulation and control of an electro-hydraulic actuated clutch, Mech. Syst. Sig. Process. 25 (2011) 1911–1922.
[40] İ. Aydoğdu, A. Akın, M.P. Saka, Design optimization of real world steel space frames using artificial bee colony algorithm with levy flight distribution, Adv. Eng. Softw. 92 (2016) 1–14.
[41] X.H. Zeng, H.Y. Cui, D.F. Song, et al., Jerk analysis of a power-split hybrid electric vehicle based on a data-driven vehicle dynamics model, Energies 11 (2018) en11061537.